An advanced SPH model for protective constructions of debris flows adopting the modified HBP constitutive law

Zhitian Qiao · Wei Shen · Matteo Berti · Tonglu Li

An advanced SPH model for protective constructions of debris flows adopting the modified HBP constitutive law

Abstract In many catchments prone to debris flows, prevention structures such as check dams and retention basins have been installed to prevent debris flows from impacting the nearby infrastructures. The SPH model adopting the Herschel–Bulkley–Papanastasiou (HBP) constitutive law has shown good potential in modeling the interaction between debris flow and prevention structures. However, the accuracy of this model is not fully satisfactory when modeling the deposition process of debris flow, because the original HBP law is a viscoplastic model which does not consider frictional dissipation. Therefore, in this paper, we proposed a novel SPH model for analyzing the interaction between debris flow and prevention structures, by incorporating a modified HBP law with frictional dissipation into the original SPH model. The proposed model is validated by column collapse and flume benchmark experiments first and then utilized to analyze a real debris flow and its interaction with the prevention structures in the Cancia catchment in northern Italian Alps. The results of the column collapse experiment show that our model exhibits a better performance in simulating the collapse process compared with the original SPH model, and the simulation results of the sand flume test illustrate that the proposed model can accurately predict the impact force of debris flow on the prevention structure. The simulation results of the Cancia debris flow demonstrate that the check dams can dramatically diminish the discharge and the frontal flow velocity of the debris flow, and the peak impact force of debris flow generally decreases with gentler channel slope. Furthermore, various prevention structures show different interaction mechanisms with debris flows: the flat deposition platform mainly dissipates the kinetic energy of the flow, the check dam mainly reduces the peak discharge of the debris flow and intercepts the debris mass, and the retention basin at the outlet contributes to the deposition of debris flow. The proposed novel SPH model is helpful for guiding the optimization design of multiple prevention structures in debris flow gullies.

Keywords Debris flows · SPH · Numerical modeling · Check dam · Flow-structure interaction

Introduction

Debris flows are regarded as the most dangerous mass movements in mountainous areas due to their high mobility and long run-out distance. They usually destroy the nearby infrastructure and pose a significant threat to the safety of the local inhabitants. Various types of prevention structures such as check dams (Shen et al. 2020, 2019; Yu et al. 2020), rigid walls (Armanini et al. 2020; Calvetti et al. 2017; Faug 2015), flexible barriers (Liu and Liang 2022; Ng et al. 2017b; Tan et al. 2019), and filter dams (Huang et al. 2007) have been installed along the debris flow gullies to mitigate the potential risk from debris flows. A key parameter for designing these structures is the peak impact force of debris flow acting on the structures (Lei et al. 2018; Li et al. 2020a, b; Scheidl et al. 2013). However, this parameter is difficult to obtain because of the complexity of the impact pro-cess of debris flow (Ma and Zhang 2007).

Limited field data related to the impact force of debris flow are available, owning to the difficulties in monitoring real debris flows and their interaction with defense structures (Hong et al. 2015; Suwa et al. 1973; Wendeler et al. 2007). Therefore, physical model tests of debris flow became a popular method to study the impact process of debris flow against structures. Many researchers adopted small-scale flume tests to simulate this process (Choi et al. 2018; Cui et al. 2015; Faug et al. 2008; Huang et al. 2022a; Jiang and Towhata 2013; Moriguchi et al. 2009; Zhang and Huang 2022; Zhou et al. 2018). Although these small-scale tests are simple and convenient for engineering purposes, they inevitably suffer from the size effect. To reduce the influence of size effect, centrifuge flume tests have been carried out to investigate the impact of different geophysical flows on the mitigation measures (Ng et al. 2019, 2017b; Song et al. 2018, 2017; Zhang and Huang 2022; Zhang et al. 2022), but the test conditions of the centrifuge tests are still too simple and are very different with the real debris flows. By contrast, numerical modeling is an efficient alternative, due to its low cost and high capacity in simulating complex conditions. Currently, full 3D models such as the Discrete Element Method (DEM) (Calvetti et al. 2017; Ng et al. 2017a; Shen et al. 2018; Zhang and Huang 2022), Smoothed Parti-cle Hydrodynamics (SPH) method (Dai et al. 2017; He et al. 2018; Huang et al. 2022b; Sheikh et al. 2021), and Material Point Method (MPM) (Cuomo et al. 2021; Li et al. 2020a, b; Li et al. 2018; Mast et al. 2014) have been applied in studying the interaction between flow-type mass movements and structures. Among these models, DEM is more suitable for simulating dry granular flows, and MPM is mainly devised for solving continuous solid mechanics problems (Jiang et al. 2016; Zhang and Huang 2022). In comparison, the SPH models have been widely applied in analyzing the dynamic process of plastic or viscoplastic flows and have shown good potential in modeling flow-structure interaction problem (Dai et al. 2017; Han et al. 2019).

One key issue limiting the capacity of the SPH method in simu-lating debris flow is the rheology law adopted in current SPH mod-els. The Bingham law is firstly incorporated into the SPH model to simulate debris flows (Dai et al. 2017; Ulrich et al. 2013). However, a numerical divergence problem will arise when the shear strain rate $\dot{\gamma}$ in the Bingham law approaches to 0. Additionally, this model

cannot simulate the shear thinning and shear thickening behavior of debris flows because it assumes a linear relationship between shear stress and shear strain rate. Therefore, the HBP constitutive law is commonly adopted to avoid the abovementioned problems. Although the SPH models adopting the HBP law show better performance in simulating the propagation and impact process of debris flows than the SPH models using the Bingham law, the simulated deposit of debris flow is generally much thinner than the real case because the frictional dissipation of debris flow is not considered in the original HBP law. To overcome this limitation, in this paper we proposed a novel SPH model by incorporating a modified HBP law which accounts for the friction dissipation of debris flow to improve the capability of the SPH models in simulating the debris flow-structure interaction problems.

The rest part of this paper is organized as follows. In "Methodology" we briefly introduced the governing equations and the modified rheological law of the proposed SPH model. Then, two benchmark tests are used to validate our model in "Validation of the model". In "Case study of the Cancia debris flow event", the model is applied to simulate a real debris-flow event that occurred in the Cancia catchment in the northern Italian Alps, and the behavior of different types of prevention structures is discussed in "Discussion". Finally, the conclusions are presented in "Conclusion".

Methodology

Governing equations

Debris flows are treated as weakly compressible fluids in this paper. The mass balance and momentum equations of the flow can be expressed as

$$\frac{d\rho}{dt} = -\rho\nabla\cdot\boldsymbol{u} \tag{1}$$

$$\frac{d\boldsymbol{u}}{dt} = -\frac{1}{\rho}\nabla p + \frac{1}{\rho}\nabla\cdot\boldsymbol{\tau} + \boldsymbol{g} \tag{2}$$

where $\boldsymbol{u}$ is the velocity vector of the flow, ρ is the density of the flow, p is the pressure, $\boldsymbol{\tau}$ denotes the shear stress tensor, and $\boldsymbol{g}$ is the gravity acceleration.

In the SPH scheme, the fluids are discretized as a series of particles. All physical quantities, such as position, velocity, density, and pressure, can be estimated using an interpolation method. Therefore, the governing equations above can be expressed in the following discrete form:

$$\frac{d\rho}{dt} = \rho_i\sum_j\frac{m_j}{\rho_j}\left(\mathbf{u}_i-\mathbf{u}_j\right)\cdot\nabla_i W_{ij} + \delta h c_0 D_i \tag{3}$$

$$\begin{aligned}\frac{d\mathbf{u}}{dt} = &-\sum_j m_j\left(\frac{p_j+p_i}{\rho_i\rho_j}\right)\cdot\nabla_i W_{ij} + \mathbf{g}\\ &+\sum_j m_j\left(\frac{\tau_j+\tau_i}{\rho_i\rho_j}\right)\cdot\nabla_i W_{ij}\end{aligned} \tag{4}$$

The last term on the right-hand side of Eq. (3) is the diffusive term, which was designed to stabilize the density field from high-frequency oscillations. c_0 is the sound velocity (assumed to be a constant), δ is a free parameter, and D_i is the indication of the dif-fusive term. Several D_i functions are available in the SPH model, such as the simplest artificial diffusion proposed by Molteni and Colagrossi 2009 and other correction formulations (Antuono et al. 2010; Fourtakas et al. 2019).

In Eq. (4), the first term on the right side represents the balanced form of the pressure term, and the last term denotes the discrete scheme of the shear stress, which will be introduced in detail in "Constitutive equation".

Under the weakly compressible assumption, the equation of state (EoS) is given by

$$P = \frac{C_S^2\rho_0}{\gamma}\left[\left(\frac{\rho}{\rho_0}\right)^{\gamma}-1\right] \tag{5}$$

where ρ_0 is the reference density, which is 1000 kg/m^3 for the water. In our case, we use $\rho_0 = 2000$ kg/m^3 to represent the debris flow density. C_s is the speed of sound estimated by $\overline{\beta\cdot g h_{\max}}$, and the recommended value of the constant β is 10 (Marrone et al. 2013; Monaghan 2000); γ is a dimensionless constant that is generally suggested to be 7 (Monaghan 2000).

Constitutive equation

Debris flow rheological laws

According to previous studies, the non-Newtonian rheological laws (such as Bingham law, HB law, and HBP law) are more suitable for modeling debris flows than the Newtonian rheological laws (Rickenmann et al. 2006; Shieh et al. 1996). Many previous studies related to SPH simulation mainly adopted the Bingham law to simulate the rheology of debris flow (Dai et al. 2017; Komatina and Jovanovíc, 1997; Monaghan 1994; Ulrich et al. 2013; Uzuoka et al. 1998). The Bingham law assumes that the flow-like movement begins only if the shear stress is larger than a critical value (i.e., the yield strength τ_y); otherwise, the material behaves like a solid. The expression of the shear stress $\boldsymbol{\tau}$ is

$$\boldsymbol{\tau} = \left(\mu + \frac{\tau_y}{2|\dot{\boldsymbol{\gamma}}|}\right)\dot{\boldsymbol{\gamma}} = \mu_{\text{eff}}\dot{\boldsymbol{\gamma}} \tag{6}$$

where $\dot{\boldsymbol{\gamma}}$ is the shear strain rate tensor, $|\dot{\boldsymbol{\gamma}}|$ is the magnitude of the shear strain rate tensor, μ is the dynamic viscosity of the material with the unit Pa • s , τ_y is the yield strength of the material, and μ_{eff} is the effective coefficient (Uzuoka et al. 1998).

According to Eq. (6), the effective viscosity will approach to infinity when the shear rate tends to 0, which may lead to numerical divergence problem. Additionally, the linear relation-ship assumption between the shear stress and shear rate is inap-propriate for debris flow. In fact, due to the complexity of their compositions, debris flows always exhibit either dilatancy or pseudo-plasticity (Major and Pierson 1992; Parsons et al. 2001; Pudasaini 2011). Therefore, the Herschel–Bulkley (HB) model was proposed (Pasculli et al. 2013). In the HB model, the effective viscosity is given by

$$\mu_{\text{eff}} = \mu|\dot{\boldsymbol{\gamma}}|^{n-1} + \frac{\tau_y}{2|\dot{\boldsymbol{\gamma}}|} \tag{7}$$

One extra parameter n is embedded into the equation in comparison with the Bingham model. Particularly, the HB model reduces to the Bingham model when $n = 1$. Although this rheological law can more accurately predict the deformation behavior of debris flow, it still cannot avoid the numerical divergence problem. For this reason, Papana-stasiou (1987) introduced another constant coefficient m into Eq. (7).

$$\mu_{\text{eff}} = \mu|\dot{\boldsymbol{\gamma}}|^{n-1} + \frac{\tau_y}{2|\dot{\boldsymbol{\gamma}}|}\left[1 - e^{-m|\dot{\gamma}|}\right] \tag{8}$$

The Herschel–Bulkley–Papanastasiou (HBP) law (Eq. 8) is always convergent because it is continuous and does not exhibit a discontinuity at $\tau = \tau_y$. For $n = 1$ and $m = 0$, the HBP model reduces to describe the Newtonian fluid. As $m \to \infty$, the HBP model can approximately represent the HB model and is further transformed into the Bingham model when $n = 1$. Overall, the HBP law is a general rheological law which can represent a variety of fluids by adopting different m and n values. The flow can behave as a shear-thinning fluid ($n < 1$) or a shear-thickening fluid ($n > 1$).

A modified HBP model considering the material friction

The yield shear strength τ_y is a constant in HBP law. However, for geo-materials, τ_y should be pressure-dependent. Therefore, in this study, we use the Mohr–Coulomb criterion to calculate the τ_y in HBP model so that the modified HBP model could simulate the frictional dissipation of debris flow. The failure envelope can be written in terms of pressure p and the second invariant of deviatoric stress J_2:

$$\sqrt{J_2} = p\sin\varphi + c\cos\varphi \tag{9}$$

where φ and c denote the internal friction angle and the cohesion of the material. The geo-material starts to yield when a critical value of shear stress τ_y is reached.

$$\sqrt{J_2} = \tau_y \tag{10}$$

Combining Eq. (9) with Eq. (10), the yielding stress τ_y of a geo-material which yields under the Mohr–Coulomb criterion can be expressed as

$$\tau_y = p\sin\varphi + c\cos\varphi \tag{11}$$

Substituting the above equation into Eq. (8), the effective viscos-ity can be expressed as

$$\mu_{\text{eff}} = \mu|\dot{\boldsymbol{\gamma}}|^{n-1} + \frac{p\sin\varphi + c\cos\varphi}{2|\dot{\boldsymbol{\gamma}}|}\left[1 - e^{-m|\dot{\gamma}|}\right] \tag{12}$$

Negative pressures will appear when using the EoS to determine the pressure based on particle density. In this study, the positive pressures $p_+ = \max\{0, p\}$ are used. Thus, the modified HBP law is given by

$$\boldsymbol{\tau} = \left\{\mu|\dot{\boldsymbol{\gamma}}|^{n-1} + \frac{p_+\sin\varphi + c\cos\varphi}{2|\dot{\boldsymbol{\gamma}}|}\left[1 - e^{-m|\dot{\gamma}|}\right]\right\}\dot{\boldsymbol{\gamma}} \tag{13}$$

This novel rheological law can mimic a variety of fluids by chang-ing the parameters (c, φ, m, n). When c, φ and m equal to 0 and $n = 1$, the law describes the Newtonian fluid, while it describes the Bing-ham-type fluid (purely cohesive material) when $\varphi = 0$ and $c \neq 0$.

Validation of the model

Two benchmark tests are used to validate the proposed model. The first one is the column collapse test conducted by Bui et al. (2008) which has been widely used to test the accuracy of numerical mod-els in predicting the movement of frictional material (Peng et al. 2021; Solowski and Sloan 2015; Zhang et al. 2021). The second one is the sand flume experiment conducted by Moriguchi et al. (2009), which is usually used to validate the numerical models for simulat-ing the dynamic impact of debris flow against structures (Cuomo et al. 2021; Dai et al. 2017; Peng et al. 2021).

Simulation of the column collapse test

In the experiment of Bui et al. (2008), small aluminum bars with a length of 50 mm and a diameter of 1 mm or 1.5 mm were used to form a rectangular region (200 mm × 100 mm × 50 mm) that simu-lates a soil column. The column collapse was triggered

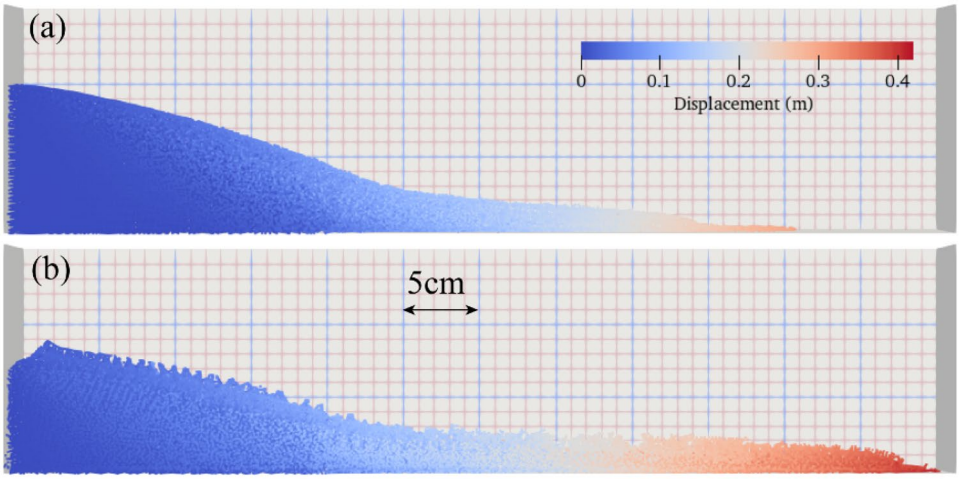

Fig. 1 The simulation results of column collapse test of **a** the modified SPH model and **b** the original HBP-based SPH model

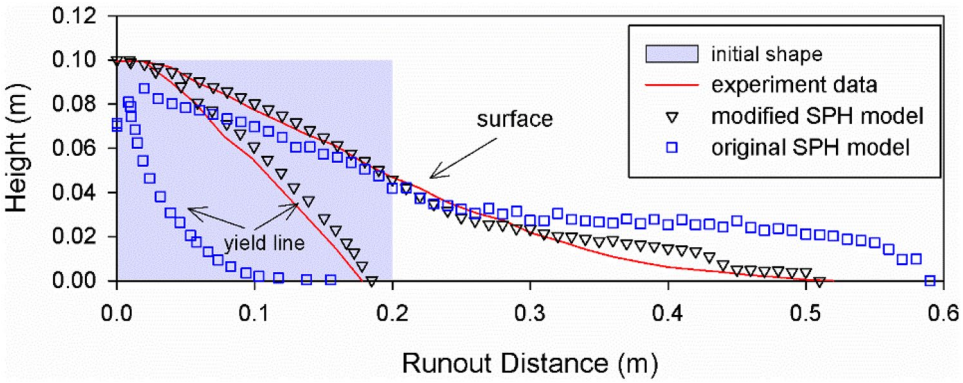

Fig. 2 Final surface height profile and yield lines in experiment and simulation

This experiment was simulated by our modified SPH model and the original HBP-based SPH model. In both simulations, the soil col-umn was modeled by 64,000 fluid particles with an initial particle spacing of 2.5 mm. Based on the results of four shear box tests on alu-minum bars (Bui et al. 2008), the following material parameters were used in our modified SPH model: density $\rho = 2650\text{kg/cm}^3$, internal friction angle $\varphi = 19.8°$, and cohesion $c = 0$ kPa. Substituting the average pressure obtained in the modified SPH model and the shear strength parameters (φ, c) above into Eq. (11), the yield shear stress

τ_y is estimated to be 0.36 kPa in the original HBP-based SPH model.

The simulation results are shown in Fig. 1 and compared with the experiment results in Fig. 2. It shows that the numerical results obtained by our modified SPH model match well with the experi-mental results not only in terms of the height profile of the deposit but also the yield lines inside the column (Fig. 2). In comparison, due to lack of friction in the original HBP-based SPH model, the material moves faster after collapse, resulting in a greater hori-zontal travel distance and a flatter deposition profile. Overall, our model shows good capability in simulating the frictional flow.

Simulation of the sand flume test

In the sand flume tests conducted by Moriguchi et al. (2009), sand columns (50 kg sand in each test) were released from a box

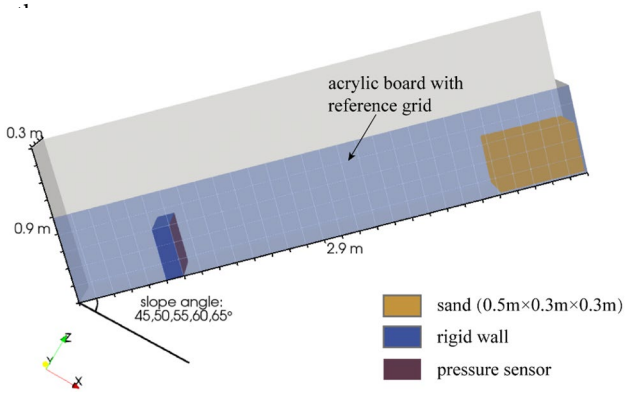

Fig. 3 Schematics of the sand flume experiment of Moriguchi et al. (2009)

flumes with different slope angles, and the run-out process of the sand flows and their impact process with the load cell were recorded (Fig. 3). This experiment was simulated by our modified SPH model. The initial interparticle distance was 0.005 m, and con-sequently, 290,675 fluid particles and 270,529 boundary particles participated in the simulation.

The flume test with a slope angle of 45° was used to calibrate the rheological parameters using the free surfaces of the sand in this test at four different times (0.4, 0.8, 1.2, and 1.6 s) provided in Moriguchi et al. (2009). The simulation results using the parameters listed in Table 1 fit well with the experimental data (Fig. 4). Adopt-ing these rheological parameters, we conducted the simulations with flume angle of 50°, 55°, 60°, and 65° to investigate the impact process of sand flow against the structure. The simulated impact forces and the experimental results are shown in Fig. 5. It shows that the simulation results are consistent with the impact force curves obtained from the experiments, demonstrating the good applicability of our model in studying the granular flow-structure interaction problems.

Case study of the Cancia debris flow event

Introduction of the July 23 debris flow event

The July 2015 Cancia debris-flow event was selected as field case to investigate the effect of prevention structures on the propagation of a natural debris flow. The Cancia catchment (Qiao et al. 2023) is located in the Dolomites region of the northern Italian Alps (Fig. 6). The outlet of the catchment is near to the Cancia village. This catchment area is

Parameters	Notion	Unit	Value
Coefficients in HBP law	m	/	100
	n	/	1.05
Fluid density	ρ	kg/m^3	1379
Dynamic viscosity	μ	Pa • s	0.02
Internal friction angle	φ	°	35
Cohesion	c	kPa	0

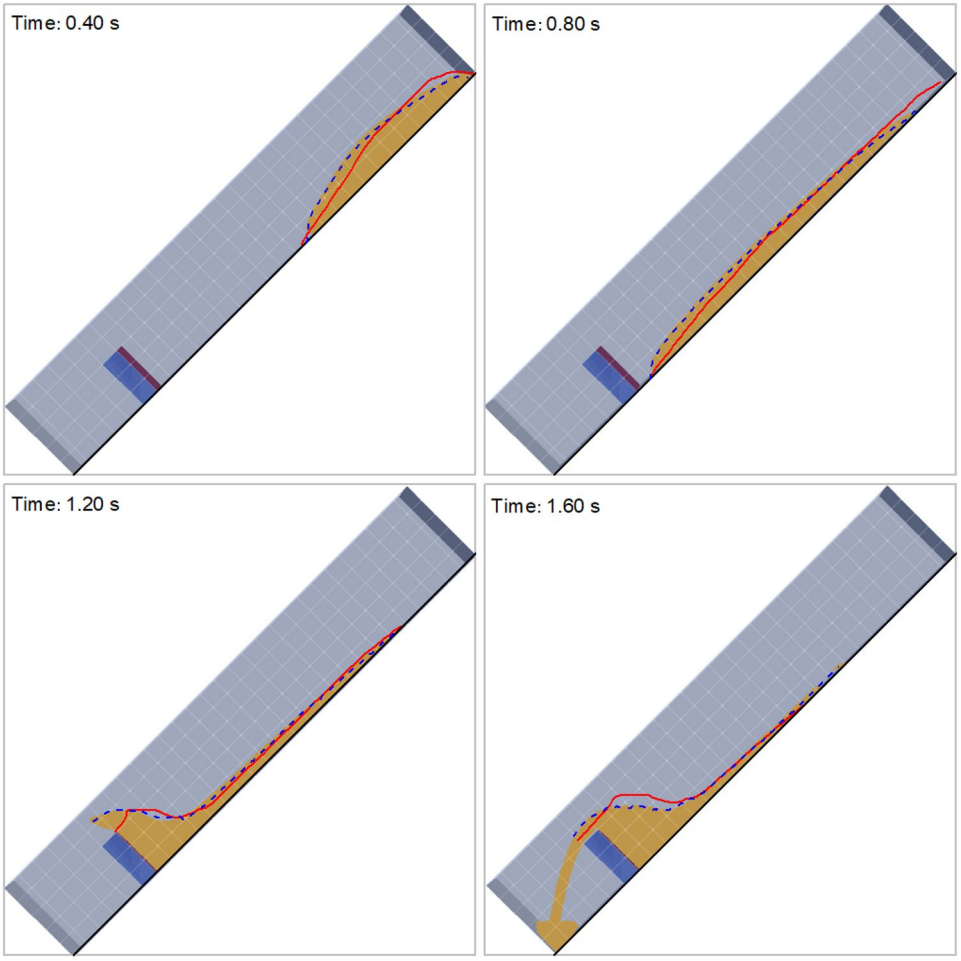

Fig. 4 Simulation results of the sand flume tests inclined at 45° of the modified SPH model (red lines represent the experiment results)

composed of two subbasins: the Salvela basin (0.65 km^2) and the Bus de Diau basin (0.99 km^2). Over 27% area of the Salvela basin is covered by vegetation. The area ratio of bare screes in the basin is 22%, which provide a large amount of source materials for debris flows.

The July 2015 debris flow was triggered by a heavy rainfall with a maximum intensity of 106 mm/h. A small amount of the debris mass accumulated in a flat deposition area build in the upper part of the channel (zone A in Fig. 7), while most parts continued to flow downward. A large portion of the debris flow was intercepted by the check dam (Dam 3 in Fig. 7) located at the channel outlet, and the rest surpassed the check dam and deposited in the lower retention basin (zone C in Fig. 7). The debris flow channel can be divided into three regions: the initiation region, propagation region, and deposition region according to the deposition characteristics of the debris flow (Fig. 7). The total run-out distance of this debris flow was approximately 2200 m (Qiao et al. 2023; Simoni et al. 2020).

Simulation settings

A digital elevation model with a resolution of 1.0 m was used to build up the 3D topography of the study area. The debris flow (total volume is 28,850 m^3) was discretized into 79,029 fluid particles. The computational region was 2131 m long in the x direction and 1663 m wide in the y direction. The maximum time step for simu-lating this case was 0.02 s. Eight groups of simulations G0–G7 were carried out to study the influence of check dams (Dam 1–Dam 3 in Fig. 7) on the propagation and deposition process of the debris flow (Table 2). Dam 3 corresponds to the check dam at the outlet of the channel which was constructed before the July 2015 debris flow event. Dam 1 and Dam 2 are two imaginary check dams which are used to investigate the influence of check dam locations on the propagation of debris flow, in which the location of Dam 1 cor-responds to that of a small check dam constructed in 2020 (P4 in Fig. 6c). The height of each dam is 8 m in these simulations. Mean-while, three cross sections (S1, S2, and S3 in Fig. 7) were selected to investigate the effect of the check dam on the discharge of the debris flow.

The main parameters used in these simulations are listed in Table 3. Among them, the initial values of the five key coeffi-cients in the HBP law (m, n, μ, φ, c) were first selected based on the parameters adopted in a study area with similar geological condi-tions (Armento et al. 2008) and then calibrated by simulation G3 (Table 2) to fit the observation results of the debris flow event.

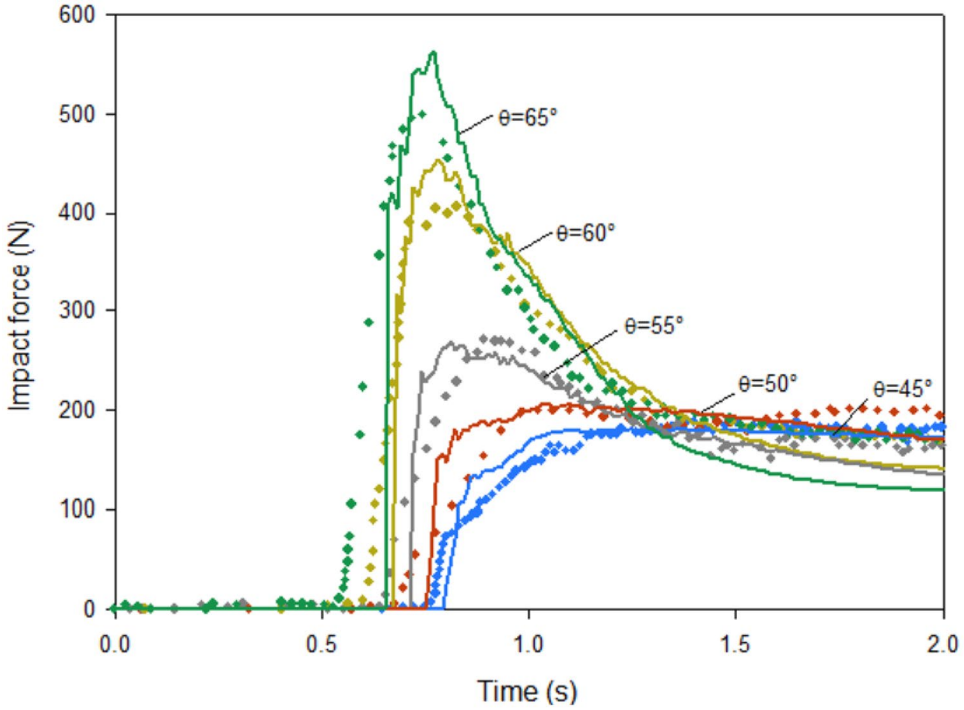

Fig. 5 Simulated and the experimental results of the impact forces in different flume dip angle conditions (solid lines represent simulation results and dots represent experimental results)

Simulation results

Run-out characteristics of the July 23 debris flow event

The simulated velocities and distributions of the July 23 debris flow event at different times are shown in Fig. 8. Overall, the simulated run-out distance and inundated area of the sediments in case G3, which represents the field conditions at the time of the event, agree well with the field observations (Simoni et al. 2020). The simu-lated maximum average velocity of the flow front is approximately 23 m/s. At around 38 s, the flow front reaches the upper flat depo-sition area. And part of the debris mass deposits here. The rest of the material continues downstream and the front of the debris flow reaches Dam 3 at approximately 260 s. Then, the flow impacts the dam, and a great amount of debris mass is intercepted by the dam. Finally, after around 30 s, the debris flow surpasses Dam 3 and accumulates in the retention basin.

Further details on the run-out characteristics of the debris flow, average velocity, and displacement of the flow front are presented in Fig. 9. As can be seen, the prevention structures in the main channel (i.e., the flat deposition area, Dam 3 and the retention basin) have significant influences on the run-out process of this debris flow. As the flow front approaches these structures, the flow front veloc-ity appears to drop sharply and the increasing of displacements becomes correspondingly slower. Additionally, the complicated 3D topography of the flow channel can cause the velocity fluctuations of the debris flow.

Influences of the check dams on the run-out process of debris flow

The simulated final depth distributions of the debris flow in different check dam conditions are shown in Fig. 10. In G0 (no check dams present), a large amount of debris mass flows past the retention basin and inundates the Cancia village. Although in G1 the final inundated area is smaller than that of G0, the prevention effect is significantly lower than that of G3, which means that only setting a check dam in the upper part of the channel may not prevent a debris flow like the July 23 event. This is probably caused by two reasons. Firstly, the width of upstream channel is narrower than downstream, and it has a relatively steeper slope than the downstream channel. Therefore, the capacity of reservoir upstream tends to be smaller. The second reason is that the velocity of flow front is relatively high when it impacts Dam 1, so more debris mass jumps over the check dam. The simulation results of G4 and G6 also indicate that check dams constructed downstream are more effective than those constructed upstream. The average deposition thickness in the retention basin in G3, G6, and G7 is about 0.8 m, 1.7 m, and 2.4 m less than that in G0. This illustrates that the prevention effect could be enhanced by building multiple dams along the flow path.

Three cross sections (S1, S2, and S3 in Fig. 7) just downstream of the check dams (Dam 1-Dam 2-Dam 3) are selected to investigate the effect of check dam location on the discharge of the debris flow. Two characteristic parameters (the peak discharge Q_m and the time t_o when the flow front arrives at the cross section) are defined to compare the influence of the check dam on the discharge of debris

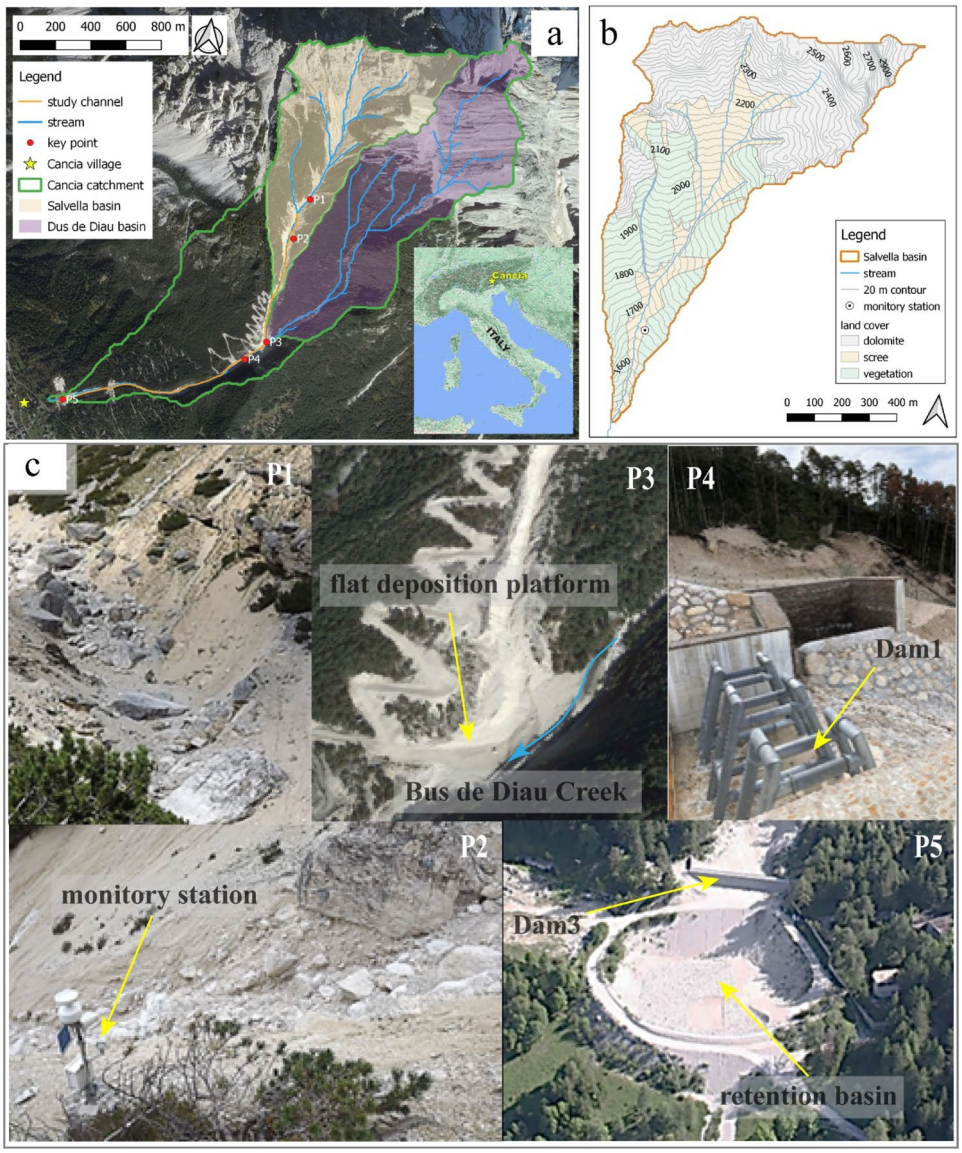

Fig. 6 **a** Overview of the Cancia catchment. **b** Schematic geomorphological features of the Salvela basin. **c** Detailed images of some key points along the channel

flows in different simulation groups. Figure 11a shows that the time
t_0 increases noticeably due to the impeding effect of Dam 1, and similar variations are only observed in S3 (Fig. 11b). Meanwhile, a peak value drop is also observed in these cases. Also in this case, the performance of Dam 3 (Fig. 11b) is significantly better than Dam 1 (Fig. 11a) because of the lower flow velocity and the gentler topog-raphy downstream. Figure 11c, d illustrates the results in the case of two and three dams along the flow path, respectively. As can be seen, the performance of multiple dams is better than that of single dam. The estimated characteristic values of all simulation groups are listed in Table 4.

A series of pressure monitoring points were set on the surface of three check dams to record the average impact pressure of debris flow on the check dam. The simulated impact pressures are shown in Fig. 12. The impact pressure curves at the three dams are very different. The impact pressure curves of Dam 1 and Dam 2 consist of obvious three stages (acceleration, deceleration, and stabilization stages), while the deceleration stage of the impact pressure curves at Dam 3 is not obvious. Additionally, the acceleration limb and the deceleration limb of Dam 2 are significantly gentler than those of Dam 1. These results suggest that the check dams in upstream are likely to suffer from higher impact force, and this is because the flow velocity in upstream of the channel is relatively larger than that downstream. Furthermore, it also shows that the upstream check dam can slightly reduce the peak impact pressure of the debris flow acting on the downstream check dam.

Discussion

The simulation results unambiguously demonstrate the signifi-cant effectiveness of check dams in reducing the flooded area, debris flow speed, and peak discharge. In Cancia, these structures

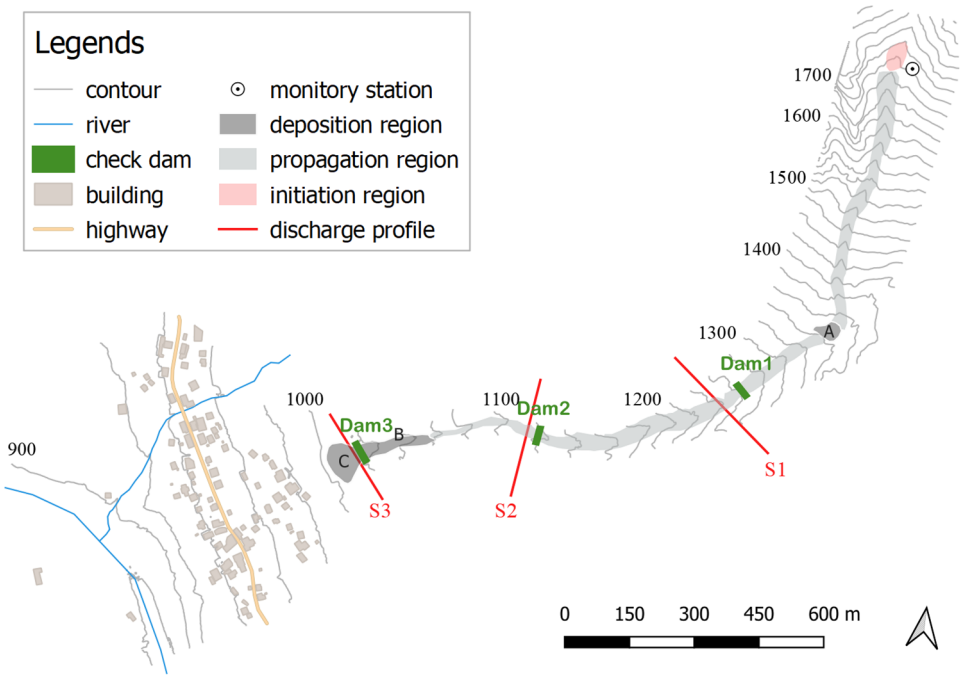

Fig. 7 Layout of the Cancia debris-flow channel and the locations of the check dams and discharge monitoring profiles in simulations

were employed in conjunction with other preventative measures, such as a flat deposition area and a retention basin, to achieve optimal results. The use of multiple structures in debris flow basins is a common practice to effectively mitigate risks. In order to investigate the interaction mechanisms of these structures on the propagation of debris flow, we carried out additional numeri-cal flume tests in eight different conditions. The schematic dia-gram of the numerical tests is shown in Fig. 13. P1 and P2 are the locations along the flow path where prevention structures may be installed, while the simulation setups are listed in Table 5.

In these simulations, the SPH particle spacing was 0.01 m, cor-responding to 35,235 flow particles. The density of the debris flow was 2000 kg/cm^3, and the other parameters used in the simula-tion are listed in Table 6. The yield stress τ_y used in the original SPH model was calibrated by ensuring that the flow reaches the outlet of the flume at the same time as the modified SPH model.

Simulation groups	Check dam settings
G0	Without check dam
G1	Dam 1
G2	Dam 2
G3	Dam 3
G4	Dam 1, Dam 2
G5	Dam 1, Dam 3
G6	Dam 2, Dam 3
G7	Dam 1, Dam 2, Dam 3

Performance of the modified SPH model in simulating debris flow deposition

The original SPH model and the modified SPH model are used to simulate the run-out process of a numerical debris flow test in condition C1. The simulated final flow depths are shown in Fig. 14.

Table 3 The main parameters run in the simulation of July 23, 2015, debris-flow event

Parameters	Notion	Unit	Value
Fluid density	ρ	kg/m^3	2000
Interparticle distance	d_p	m	0.7
Number of fluid particles	N_{pf}	/	79,029
Number of boundary particles	N_{pb}	/	2,083,275
Simulation duration	t	s	450
Initial time interval	Δt	s	0.012
Coefficients in HBP law	m	/	0.15
	n	/	1.05
Dynamic viscosity	μ	Pa • s	97
Internal friction angle	φ	°	20
Cohesion	c	kPa	4

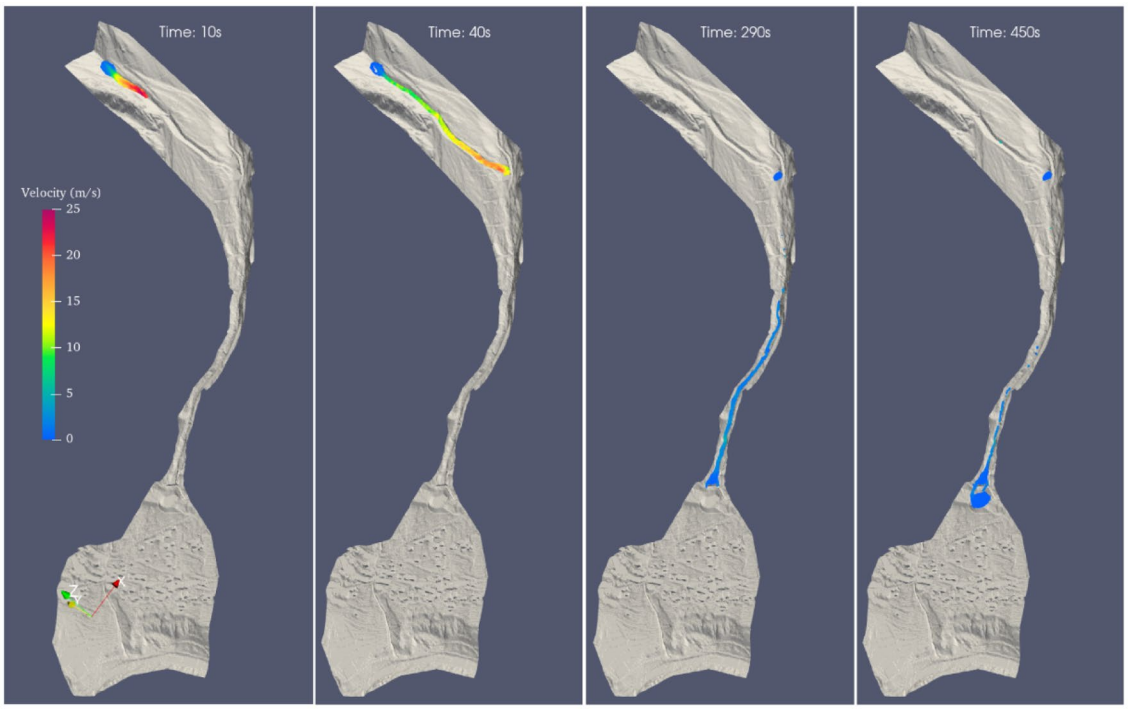

Fig. 8 The simulated propagation process of July 23, 2015, debris flow

It shows that deposit of the debris flow simulated by the original SPH model is thinner and flatter than that simulated by our modified SPH model. The flat deposition platform stops more debris mass in the modified SPH model. The simulation results of the modified SPH model fit better with the real debris flow in which the frictional dissipation in the flow is non-ignorable.

Influence of different structures on debris flow propagation

The average velocity of the flow front and the discharge of the flow at the outlet of the flume in Co–C2 are illustrated in Fig. 15. Results show that both the flat deposition area and check dam contribute to decreasing the kinetic energy of the flow and

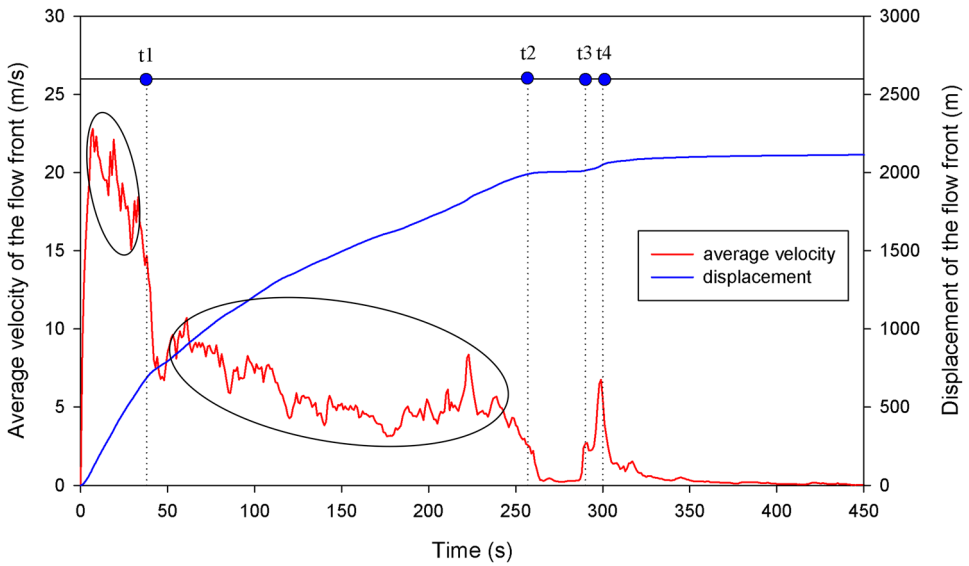

Fig. 9 Average velocity and displacement of the flow front in G3 simulation (*t*1, *t*2, and *t*4 are the time when the debris flow reaches the flat deposition platform, Dam 3, and the retention basin, respectively; *t*3 is the time when the debris flow surpasses over Dam 3)

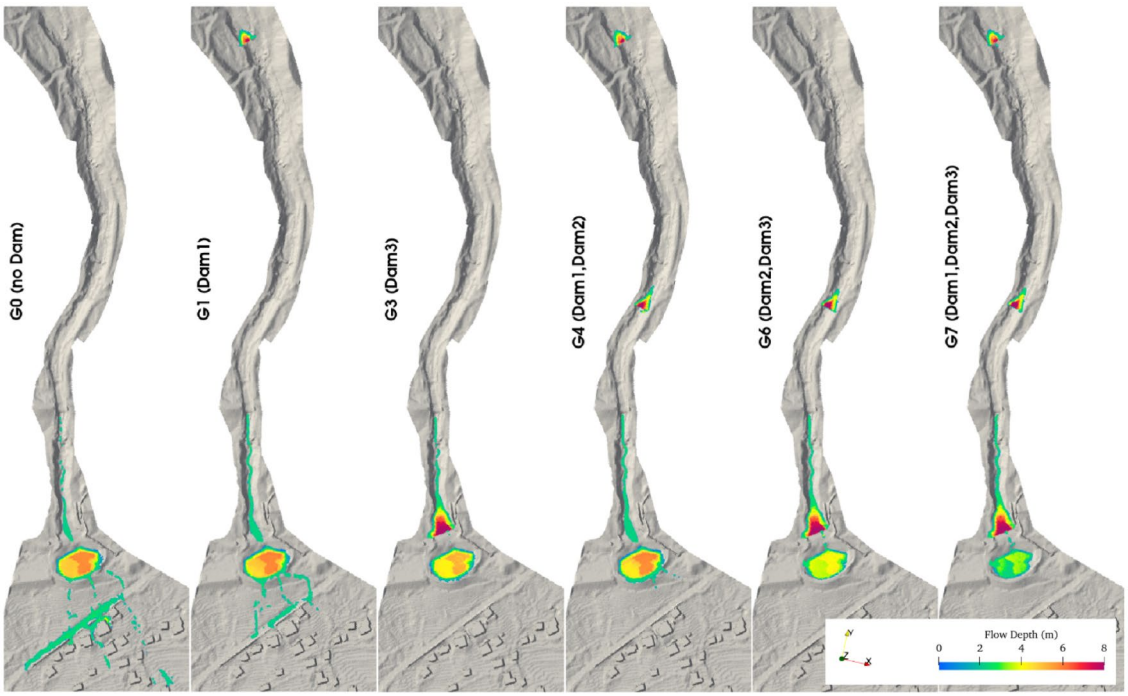

Fig. 10 Comparison of the final flow depth distributions in different simulation groups

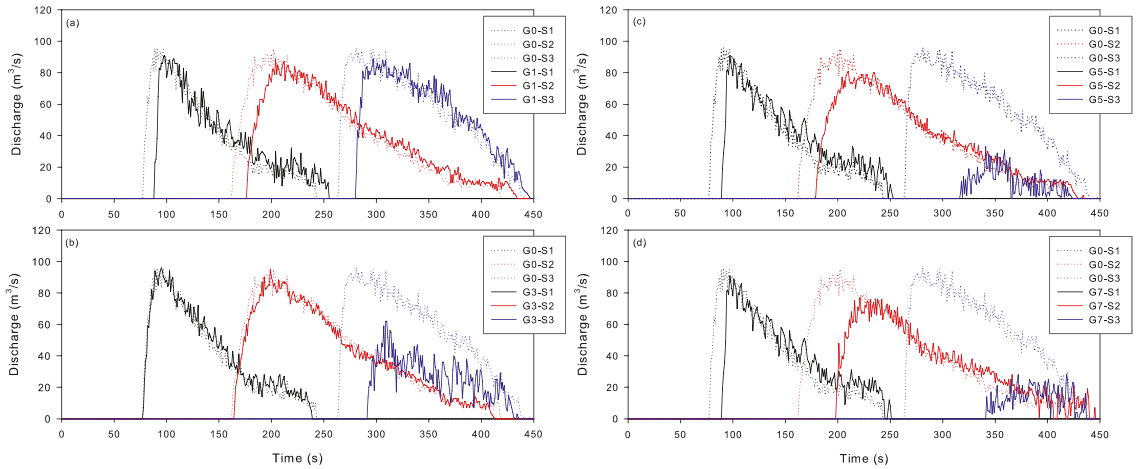

Fig. 11 Influence of the check dam on discharge time series in three sections (S1, S2, and S3)

Table 4 The estimated characteristic values in all simulation groups

Simulation groups	The peak values Q_m (m^3/s)			The initial time t_o (s)		
	S1	S2	S3	S1	S2	S3
G0	95.866	95.061	96.009	78	163	264
G1	90.909	88.8658	88.924	89	177	281
G2	95.866	85.100	86.029	78	180	282
G3	95.866	95.021	62.096	78	165	292
G4	90.909	79.041	84.005	89	194	300
G5	90.922	81.086	32.971	90	179	317
G6	95.866	82.005	30.052	78	183	317
G7	90.922	77.094	28.048	90	199	342

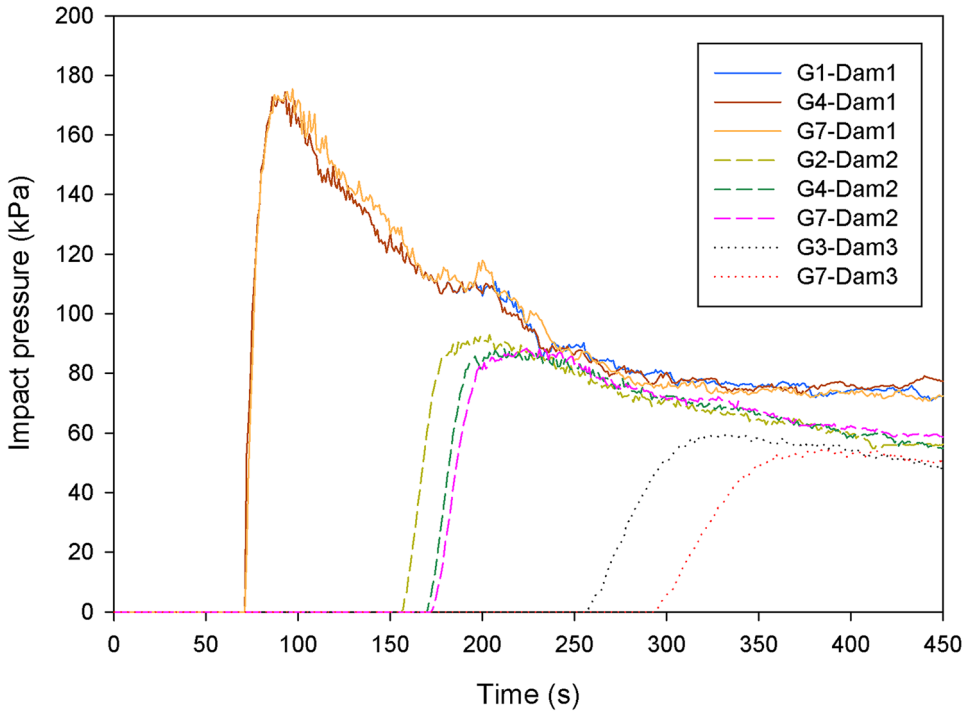

Fig. 12 The estimated impact pressure time series in the different simulation groups

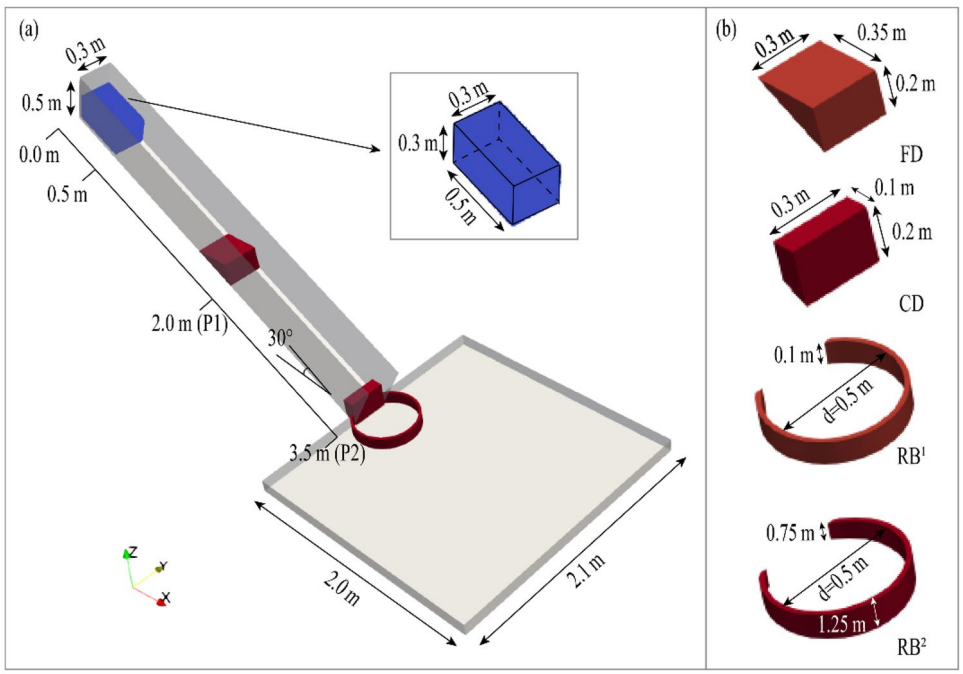

Fig. 13 Schematic diagram of **a** the flume model and **b** structures (FD: flat deposition area; CD: check dam; RB[1]: retention basin with same retaining wall height; RB.[2]: retention basin with increased retaining wall height)

Table 5 Structure settings for different simulation groups

Simulation groups	Structure settings
C0	No structure
C1	FD in P1
C2	CD in P1
C3	CD in P2
C4	RB^1 in P2
C5	RB^2 in P2
C6	FD in P1 and CD in P2
C7	FD in P1 and RB^1 in P2

FD flat deposition area, *CD* check dam, *RB* retention basin

Table 6 The main parameters in the dynamic simulation

Parameters	Original SPH model		Modified SPH model	
	Notation	Value	Notation	Value
Coefficients in HBP law	m	100	m	100
	n	1.05	n	1.05
Dynamic viscosity	$\mu(\mathrm{Pa}\cdot\mathrm{s})$	1	$\mu(\mathrm{Pa}\cdot\mathrm{s})$	1
Yield strength	$\tau_y(\mathrm{kPa})$	1.3	$\varphi(^\circ)$	28
			$c(\mathrm{kPa})$	0

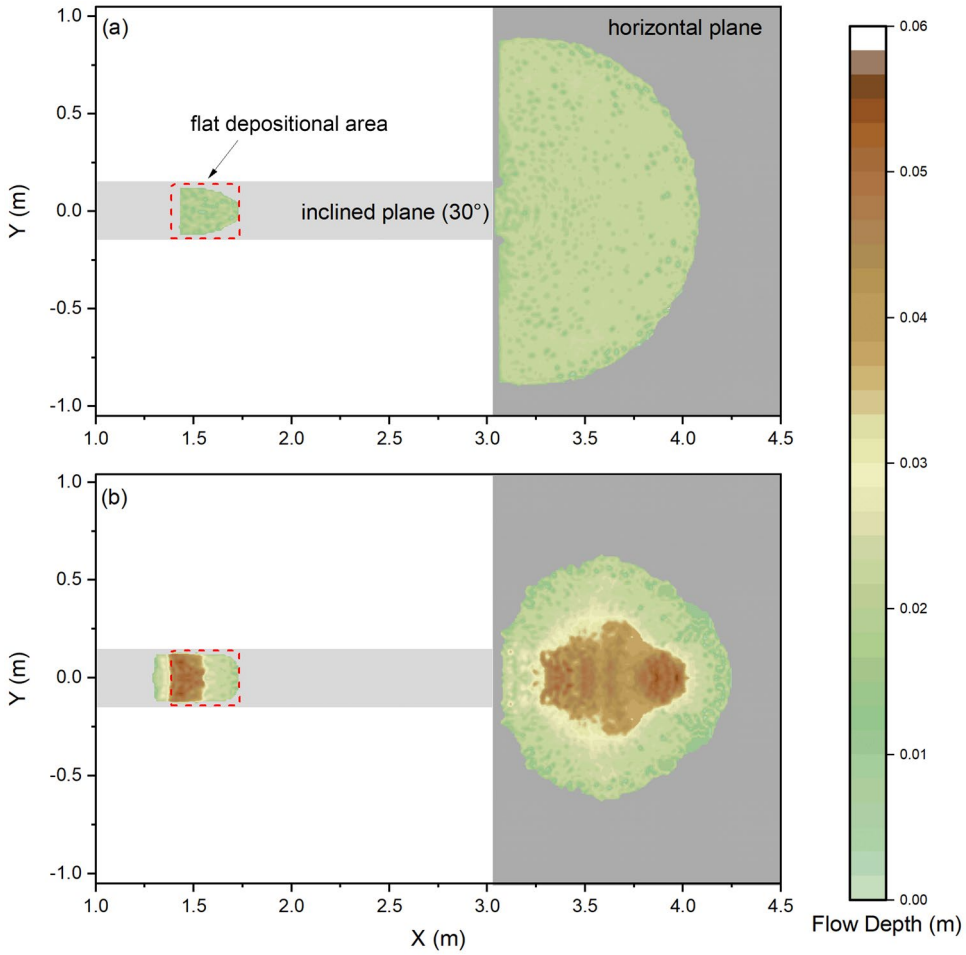

Fig. 14 Flow depth of final deposition obtained by **a** the original SPH model and **b** the modified SPH model

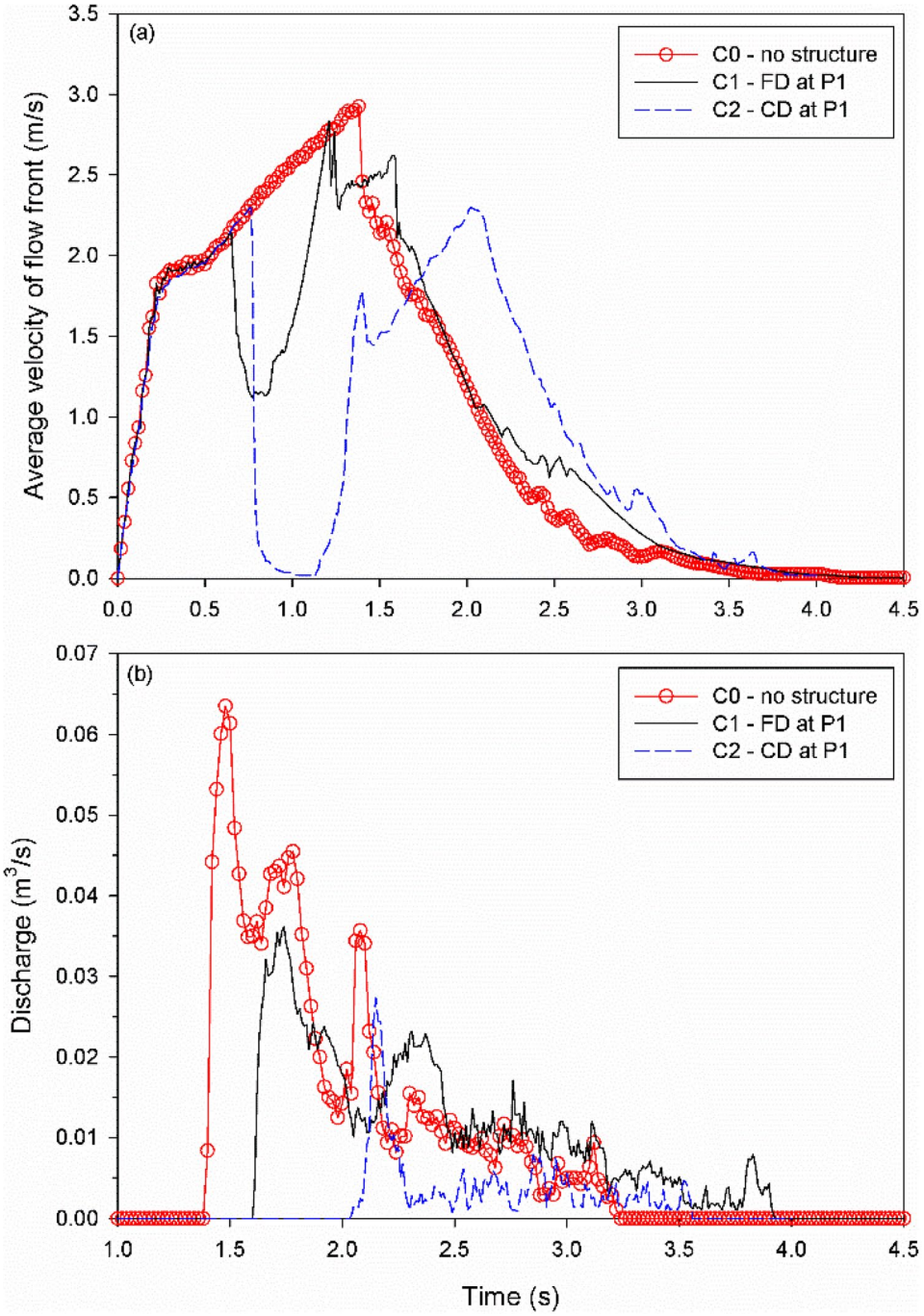

Fig. 15 **a** Average velocity of flow front and **b** discharge time series at the outlet of the flume

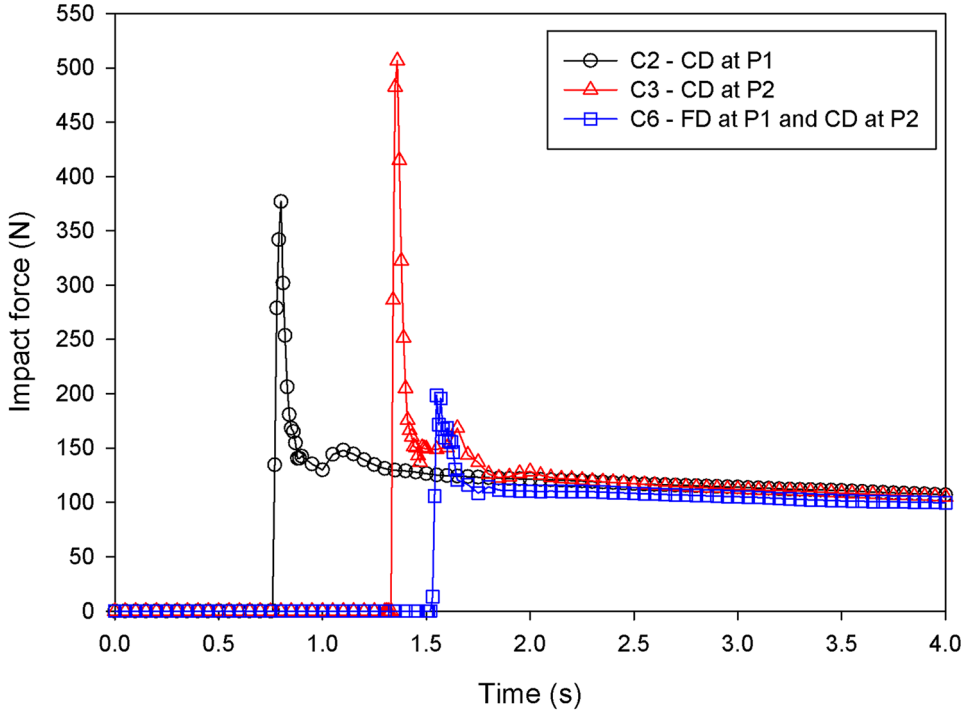

Fig. 16 Comparison of impact force time series for different simulation groups

reducing the peak discharge. The two types of structures achieve these results through different mechanisms. In a check dam (C2), the kinetic energy of the flow front is mainly lost due to the col-lision of the flow front and the dam. Meanwhile, the discharge dramatically reduces because a large amount of debris mass is intercepted by the dam. In a flat deposition area (C1), the decrease of the average velocity of the flow front is mainly caused by the friction dissipation in the flow, although a small part of the flow material deposits there.

The impact forces acting on the check dams in different simu-lation groups are shown in Fig. 16. The magnitude of impact force acting on the check dam is related to the velocity of the flow front. Since the flow is accelerating from P1 to P2 (Fig. 15a), the peak impact force of C3 is greater than that in C2. In each simulation, the impact force eventually converges to the same stable value at around 100 N. If a flat deposition platform is installed in front of the check dam (C6), part of the kinetic energy of the flow is lost before impacting the check dam. Thus, the peak impact force exerted on the check dam can be signifi-cantly reduced.

The simulated inundating areas of the groups with and without the retention basin (Co vs. C4 and C1 vs. C7) are presented in Fig. 17. It can be concluded that the retention basin has the ability to reduce the affected area and shorten the run-out dis-tance. In addition, the comparison of Co and C1 (or C4 and C7) shows that the flat deposition area also contributes to reducing the run-out of the flow front (Fig. 17b), but has little effect on the reduction of the inundating area (Fig. 17a) in the specific case considered. To further study the influence of retention basin dimension on debris flow propagation, we modified the height of the retaining wall of the retention basin as shown in Fig. 13b. Compared with the results of C4, a smaller inundated area and a shorter run-out distance are observed in simulation C5. It indicates that the improved retention basin is more effective in debris flow mitigation when the engineering quantity is simi-lar. Based on the analysis above, the main function of retention basin is to adjust the inundating area and delay the arrival time of the debris flow.

In summary, the three different structures exhibit different behavior. Each one has a significant advantage in mitigating the debris flow. Flat deposition areas are often constructed along the debris flow channel with high slopes, providing a gentler area for the flow to spread out and dissipate the kinetic energy. Check dams are mainly used to reduce debris flow intensity (peak discharge and debris flow volume). Since the impact force acting on check dams is related to the kinetic energy of the flow front. Retention basins are usually built at the outlet to reduce the impact area of the debris flow and prevent it from causing damage to downstream infrastructures. Additionally, the shape of retention basin can be designed based on the flow direction to improve its performance in mitigating debris flow.

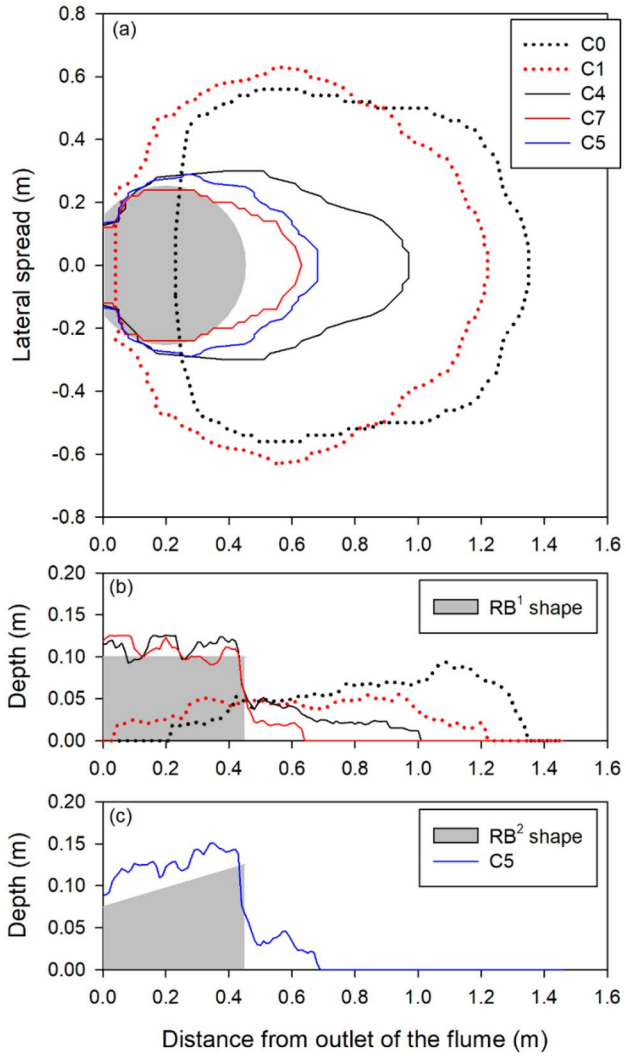

Fig. 17 Simulation results of the final debris flow deposition: **a** plan view; **b** and **c** longitudinal section

Conclusion

A novel SPH model adopting the modified HBP constitutive law was established in this paper to simulate debris flow-structure interaction. Two benchmark experiments were used to validate our model. Furthermore, a real debris-flow event was analyzed using the model and the prevention mechanisms of various structures are discussed. The following conclusions can be obtained:

(1) The simulation results of column collapse and flume experiments demonstrated that our modified model, which introduce friction into a HBP rheological law, can more accurately predict deposition process of debris flow. And the simulation results of flume experiments illustrated the effectiveness of the modified model in predicting the interaction between debris flow and structures.

(2) The simulation results of the July 23 debris-flow event in the Cancia basin (Italian Alps) show that the peak impact pressure varies with the location of check dam. The impact pressure in the upper part of the channel appears to be greater than that downstream, which can be explained by the steeper terrains and faster flow velocity upstream compared to downstream.

(3) Different prevention structures have different mechanisms when they interact with debris flows. The flat deposition platforms mainly contribute to decreasing the flow front velocity and are usually built in the upper part of the channel. The main function of check dams is to reduce the discharge downstream by intercepting the debris mass. Retention basins are often constructed at the outlet of the channel to prevent debris flows from flooding the surrounding infrastructures, and a better mitigation effect can be achieved if we consider the flow direction when designing the shape of the retention basin. Our modified SPH model has the potential to be utilized in guiding the optimization design of these prevention structures in debris flow gullies.

Acknowledgements

We would like to thank the developer team of DualsPhysics, who developed the open-source SPH code and released it to the public. We also thank the anonymous referees for carefully reading the manuscript and providing constructive comments to help us improve the quality of this paper.

Funding

This research is funded by the National Key R&D Program of China (2021YFE0111900) and the China Scholarship Council (CSC)—University of Bologna Joint Scholarship (File No. 202006560018).

Declarations

Conflict of interest The authors declare no competing interests.

References

Antuono M, Colagrossi A, Marrone S, Molteni D (2010) Free-surface flows solved by means of SPH schemes with numerical diffusive terms. Comput Phys Commun 181:532–549. https://doi.org/10.1016/j.cpc.2009.11.002

Armanini A, Rossi G, Larcher M (2020) Dynamic impact of a water and sediments surge against a rigid wall. J Hydraul Res 58:314–325. https://doi.org/10.1080/00221686.2019.1579113

Armento MC, Genevois R, Tecca PR (2008) Comparison of numerical models of two debris flows in the Cortina d' Ampezzo area, Dolomites, Italy. Landslides 5:143–150. https://doi.org/10.1007/s10346-007-0111-2

Bui HH, Fukagawa R, Sako K, Ohno S (2008) Lagrangian meshfree particles method (SPH) for large deformation and failure flows of geomaterial using elastic–plastic soil constitutive model. Int J Numer Anal Methods Geomech 32:1537–1570. https://doi.org/10.1002/nag

Calvetti F, di Prisco CG, Vairaktaris E (2017) DEM assessment of impact forces of dry granular masses on rigid barriers. Acta Geotech 12:129–144. https://doi.org/10.1007/s11440-016-0434-z

Choi SK, Lee JM, Kwon TH (2018) Effect of slit-type barrier on characteristics of water-dominant debris flows: small-scale physical modeling. Landslides 15:111–122. https://doi.org/10.1007/s10346-017-0853-4 Cui P, Zeng C, Lei Y (2015) Experimental analysis on the impact force of viscous debris flow. Earth Surf Process Landf 40:1644–1655. https://doi.org/10.1002/esp.3744

Cuomo S, Di Perna A, Martinelli M (2021) Material point method (Mpm) hydro-mechanical modelling of flows impacting rigid walls. Can Geotech J 58:1730–1743. https://doi.org/10.1139/cgj-2020-0344

Dai Z, Huang Y, Cheng H, Xu Q (2017) SPH model for fluid–structure interaction and its application to debris flow impact estimation. Landslides 14:917–928. https://doi.org/10.1007/s10346-016-0777-4

Faug T (2015) Depth-averaged analytic solutions for free-surface granular flows impacting rigid walls down inclines. Phys. Rev. E - Stat. Non-linear, Soft Matter Phys 92:1–14. https:// doi. org/ 10. 1103/ PhysRevE. 92.062310

Faug T, Chanut B, Naaim M, Perrin B (2008) Avalanches overflowing a dam: dead zone, granular bore and run-out shortening. Ann Glaciol 49:77–82. https://doi.org/10.3189/172756408787814799 Fourtakas G,

Dominguez JM, Vacondio R, Rogers BD (2019) Local uniform stencil (LUST) boundary condition for arbitrary 3-D boundaries in parallel smoothed particle hydrodynamics (SPH) models. Comput Fluids 190:346–361. https://doi.org/10.1016/j.compfluid.2019.06.009

Han Z, Su B, Li Y, Wei W, Weidong W, Huang J, Chen G (2019) Numerical simulation of debris-flow behavior based on the SPH method incorporating the Herschel-Bulkley-Papanastasiou rheology model. Eng Geol 255:26–36. https://doi.org/10.1016/j.enggeo.2019.04.013

He X, Liang D, Wu W, Cai G, Zhao C, Wang S (2018) Study of the interac-tion between dry granular flows and rigid barriers with an SPH model. Int J Numer Anal Methods Geomech 42:1217–1234. https://doi.org/10.1002/nag.2782

Hong Y, Wang JP, Li DQ, Cao ZJ, Ng CWW, Cui P (2015) Statistical probabilistic analyses of impact pressure and discharge of debris flow from 139 events during 1961 and 2000 at Jiangjia Ravine. China Eng Geol 187:122–134. https://doi.org/10.1016/j.enggeo.2014.12.011

Huang H, Yang K, Lai S (2007) Impact force of debris flow on filter dam. Eur Geosci Union Gen Assem 9:1–32

Huang Y, Jin X, Ji J (2022a) Effects of barrier stiffness on debris flow dynamic impact—I: laboratory flume test. Water (Switzerland) 14. https://doi.org/10.3390/w14020177

Huang Y, Jin X, Ji J (2022b) Effects of barrier stiffness on debris flow dynamic impact—II: numerical simulation. Water (Switzerland) 14. https://doi.org/10.3390/w14020182

Jiang C, Schroeder C, Teran J, Stomakhin A, Selle A (2016) The material point method for simulating continuum materials. In: Proceedings of the ACM SIGGRAPH 2016 Courses. pp. 1–52

Jiang YJ, Towhata I (2013) Experimental study of dry granular flow and impact behavior against a rigid retaining wall. Rock Mech Rock Eng 46:713–729. https://doi.org/10.1007/s00603-012-0293-3

Komatina D, Jovanovíc M (1997) Experimental study of steady and unsteady free surface flows with water-clay mixtures. J Hydraul Res 35:579–590. https://doi.org/10.1080/00221689709498395

Lei Y, Cui P, Zeng C, Guo Y (2018) An empirical mode decomposition-based signal process method for two-phase debris flow impact. Landslides 15:297–307. https://doi.org/10.1007/s10346-017-0864-1

Li X, Xie Y, Gutierrez M (2018) A soft–rigid contact model of MPM for granular flow impact on retaining structures. Comput Part Mech 5:529–537. https://doi.org/10.1007/s40571-018-0188-5

Li S, Peng C, Wu W, Wang S, Chen X, Chen J, Zhou GGD, Chitneedi BK (2020) Role of baffle shape on debris flow impact in step-pool channel: an SPH study. Landslides 17:2099–2111. https:// doi. org/ 10. 1007/ s10346-020-01410-w

Li X, Yan Q, Zhao S, Luo Y, Wu Y, Wang D (2020) Investigation of influence of baffles on landslide debris mobility by 3D material point method. Landslides 17:1129–1143. https://doi.org/ 10.1007/ s10346-020-01346-1

Liu C, Liang L (2022) A coupled SPH–DEM–FEM approach for modeling of debris flow impacts on flexible barriers. Arab J Geosci 15. https://doi.org/10.1007/s12517-022-09739-3

Ma S, Zhang X (2007) Material point method for impact and explosion problems. Comput Mech 156–166. https://doi.org/10.1007/978-3-540-75999-7_14

Major J, Pierson T (1992) Debris flow rheology: experimental analysis of fine-grained slurries. Water Resour Res 28:841–857

Marrone S, Colagrossi A, Antuono M, Colicchio G, Graziani G (2013) An accurate SPH modeling of viscous flows around bodies at low and moderate Reynolds numbers. J Comput Phys 245:456–475. https://doi.org/10.1016/j.jcp.2013.03.011

Mast CM, Arduino P, Miller GR, Mackenzie-Helnwein P (2014) Avalanche and landslide simulation using the material point method: flow dynamics and force interaction with structures. Comput Geosci 18:817–830. https://doi.org/10.1007/s10596-014-9428-9

Molteni D, Colagrossi A (2009) A simple procedure to improve the pressure evaluation in hydrodynamic context using the SPH. Comput Phys Commun 180:861–872. https://doi.org/10.1016/j.cpc.2008.12.004

Monaghan JJ (1994) Simulating free surface flows with SPH. J Comput Phys. https://doi.org/10.1006/jcph.1994.1034

Monaghan JJ (2000) SPH without a tensile instability. J Comput Phys 159:290–311. https://doi.org/10.1006/jcph.2000.6439

Moriguchi S, Borja RI, Yashima A, Sawada K (2009) Estimating the impact force generated by granular flow on a rigid obstruction. Acta Geotech 4:57–71. https://doi.org/10.1007/s11440-009-0084-5

Ng CWW, Choi CE, Goodwin GR, Cheung WW (2017) Interaction between dry granular flow and deflectors. Landslides 14:1375–1387. https://doi.org/10.1007/s10346-016-0794-3

Ng CWW, Song D, Choi CE, Liu LHD, Kwan JSH, Koo RCH, Pun WK (2017) Impact mechanisms of granular and viscous flows on rigid and flexible barriers. Can Geotech J 54:188–206. https://doi.org/ 10.1139/ cgj-2016-0128

Ng CWW, Choi CE, Cheung DKH, Cui Y (2019) Effects of dynamic fragmentation on the impact force exerted on rigid barrier: centrifuge modelling. Can Geotech J 56:1215–1224. https://doi.org/10.1139/ cgj-2018-0092

Papanastasiou TC (1987) Flows of Materials with Yield. J Rheol (N. Y. N. Y) 31:385–404. https://doi.org/10.1122/1.549926

Parsons JD, Whipple KX, Simoni A (2001) Experimental study of the grain flow, fluid-mud transition in debris flows. J Geol 109:427–447. https://doi.org/10.1086/320798

Pasculli A, Minatti L, Sciarra N, Paris E (2013) SPH modeling of fast muddy debris flow:numerical and experimental comparison of certain commonly utilized approaches. Ital J Geosci 132:350–365. https:// doi. org/ 10.3301/IJG.2013.01

Peng C, Bašić M, Blagojević B, Bašić J, Wu W (2021) A Lagrangian differencing dynamics method for granular flow modeling. Comput Geotech 137. https://doi.org/10.1016/j.compgeo.2021.104297 Pudasaini SP (2011) Some exact solutions for debris and avalanche flows. Phys Fluids 23. https://doi.org/10.1063/1.3570532

Qiao Z, Li T, Simoni A, Gregoretti C, Bernard M, Wu S, Shen W, Berti M (2023) Numerical modelling of an alpine debris flow by considering bed entrainment. Front Earth Sci 10:1–17. https://doi.org/ 10.3389/ feart.2022.1059525

Rickenmann D, Laigle D, McArdell BW, Hübl J (2006) Comparison of 2D debris-flow simulation models with field events. Comput Geosci 10:241–264. https://doi.org/10.1007/s10596-005-9021-3

Scheidl C, Chiari M, Kaitna R, Müllegger M, Krawtschuk A, Zimmermann T, Proske D (2013) Analysing debris-flow impact models, based on a small scale modelling approach. Surv Geophys 34:121–140. https://doi.org/10.1007/s10712-012-9199-6

Sheikh B, Qiu T, Ahmadipur A (2021) Comparison of SPH boundary approaches in simulating frictional soil–structure interaction. Acta Geotech 16:2389–2408. https://doi.org/10.1007/s11440-020-01063-y

Shen W, Zhao T, Zhao J, Dai F, Zhou GGD (2018) Quantifying the impact of dry debris flow against a rigid barrier by DEM analyses. Eng Geol 241:86–96. https://doi.org/10.1016/j.enggeo.2018.05.011

Shen W, Wang D, Qu H, Li T (2019) The effect of check dams on the dynamic and bed entrainment processes of debris flows. Landslides 16:2201–2217. https://doi.org/10.1007/s10346-019-01230-7

Shen W, Wang D, He S, Li T (2020) Numerical assessment of the impeding effect of check dams in the Hongchun debris flow gully, Sichuan Province. China Bull Eng Geol Environ 79:2833–2845. https:// doi. org/ 10.1007/s10064-020-01755-5

Shieh CL, Jan CD, Tsai YF (1996) A numerical simulation of debris flow and its application. Nat Hazards 13:39–54. https://doi.org/10.1007/ BF00156505

Simoni A, Bernard M, Berti M, Boreggio M, Lanzoni S, Stancanelli LM, Gregoretti C (2020) Runoff-generated debris flows: observation of

initiation conditions and erosion–deposition dynamics along the channel at Cancia (eastern Italian Alps). Earth Surf Process Landforms 45:3556–3571. https://doi.org/10.1002/esp.4981
Solowski WT, Sloan SW (2015) Evaluation of material point method for use in geotechnics. Int J Numer Anal Methods Geomech 39:685–701. https://doi.org/10.1002/nag
Song D, Ng CWW, Choi CE, Zhou GGD, Kwan JSH, Koo RCH (2017) Influence of debris flow solid fraction on rigid barrier impact. Can Geotech J 54:1421–1434. https://doi.org/10.1139/cgj-2016-0502
Song D, Choi CE, Ng CWW, Zhou GGD (2018) Geophysical flows impacting a flexible barrier: effects of solid-fluid interaction. Landslides 15:99–110. https://doi.org/10.1007/s10346-017-0856-1
Suwa H, Okuda S, Yokoyama K (1973) Observation system on rocky mudflow. Bull Disaster Prev Res Inst 23:59–73
Tan D-Y, Yin J-H, Feng W-Q, Zhu Z-H, Qin J-Q, Chen W-B (2019) New simple method for calculating impact force on flexible barrier considering partial muddy debris flow passing through. J Geotech Geoenvironmental Eng 145:04019051. https://doi.org/10.1061/(asce)gt.1943-5606.0002133
Ulrich C, Leonardi M, Rung T (2013) Multi-physics SPH simulation of complex marine-engineering hydrodynamic problems. Ocean Eng 64:109–121. https://doi.org/10.1016/j.oceaneng.2013.02.007 Uzuoka R, Yashima A, Kawakami T, Konrad JM (1998) Fluid dynamics based prediction of liquefaction induced lateral spreading. Comput Geotech 22:243–282. https://doi.org/10.1016/S0266-352X(98)00006-8
Wendeler C, Volkwein A, Roth A, Denk M, Wartmann S (2007) Field measurements used for numerical modelling of flexible debris flow barriers. Int Conf Debris-Flow Hazards Mitig Mech Predict Assessment Proc 681–687
Yu X, Chen X, Wang H, Jia C (2020) Numerical study on the interaction between debris flow slurry and check dams based on fluid–solid coupling theory. Geotech Geol Eng 38:2427–2445. https://doi.org/10.1007/s10706-019-01160-0
Zhang C, Yin Y, Yan H, Zhu S, Li B, Hou X, Yang Y (2022) Centrifuge modeling of multi - row stabilizing piles reinforced reservoir landslide with different row spacings. https://doi.org/10.1007/s10346-022-01994-5
Zhang B, Huang Y (2022) Impact behavior of superspeed granular flow: insights from centrifuge modeling and DEM simulation. Eng Geol 299:106569. https://doi.org/10.1016/j.enggeo.2022.106569
Zhang W, Zhong Z, Peng C, Yuan W, Wu W (2021) GPU-accelerated smoothed particle finite element method for large deformation analy-sis in geomechanics. Comput Geotech 129:103856. https://doi.org/10. 1016/j.compgeo.2020.103856
Zhou GGD, Song D, Choi CE, Pasuto A, Sun QC, Dai DF (2018) Surge impact behavior of granular flows: effects of water content. Landslides 15:695–709. https://doi.org/10.1007/s10346-017-0908-6

Zhitian Qiao · Matteo Berti
Department of Biological, Geological and Environmental Sciences, University of Bologna, Bologna 40126, Italy

Wei Shen .Tonglu Li
Department of Geological Engineering, Chang'an University, Xi'an 710064, China
Email: shenweichd@qq.com